

ON THE MICROSTRUCTURE, HARDNESS AND IMPACT TOUGHNESS OF 356 AND 413 ALLOYS

A. M. Samuel, E. M. Elgallad, and F. H. Samuel

Université du Québec à Chicoutimi, Chicoutimi, Quebec G7H 2B1, Canada

H. W. Doty

General Motors, Materials Engineering, Pontiac, MI, USA

S. Valtierra

Corporativo Nemak, S.A. de C.V., Garza Garcia, N.L., Mexico

Copyright © 2016 American Foundry Society
DOI 10.1007/s40962-016-0066-y

Abstract

The present study was performed on 356 and 413 alloys containing various amounts of hydrogen (H_2), titanium diboride (TiB_2) and strontium (Sr). The results show that the eutectic silicon particles in non-modified alloys undergo coarsening during the solutionizing treatment. A new mechanism, based on the Ostwald theory, has been proposed to explain the observed phenomenon. Although the variation in melt treatment parameters has no significant influence on the alloy hardness, it does have a great effect on the alloy impact toughness. Best results are obtained when the alloy is degassed, Sr-modified and grain refined. Also, Sr-modified, degassed 413 alloys have been found to possess good impact toughness. Precipitation of

Mg_2Si phase particles in 356 alloy is more effective as a hardening agent than the Al_2Cu phase precipitated in the 413 alloy. The increased Si content in non-modified 413 alloys accelerates crack initiation and propagation, leading to low toughness values. Modifying the 413 alloys with 200 ppm Sr results in a more even distribution of the spheroidized eutectic Si particles and hence improves the alloy toughness.

Keywords: aluminum alloys, melt treatment, heat treatment, hardness, impact toughness

Introduction

The Charpy impact test is a popular test for measuring the toughness of materials; it should be remembered, however, that it was developed before the theory of fracture mechanics was formulated.¹ The total absorbed energy required for breaking the material is measured by the high strain rate fracture of a standard notched or unnotched specimen.² The total absorbed energy dissipated in breaking the test specimen is then measured based on the difference in the potential energy of the striking pendulum.³ Also, the total absorbed impact energy may be represented by the area located under the load–time curve which is obtained from an instrumented Charpy impact testing machine.⁴ In the presence of a notch, the impact energy will be much lower than that in the case of an unnotched specimen. The unnotched impact specimen provides highly

accurate results, drawing attention to the fact that the impact values depend on the microstructure rather than on the specimen configuration.²

During the past ten years, the research group at the Université du Québec à Chicoutimi has carried out an intensive program on the parameters that control the toughness of aluminum alloys and their composites using unnotched samples.^{5–10} The main results inferred from these studies show that the Sr-modified alloys exhibit higher levels of impact values for all aging times used at 220 °C (428 °F) than those obtained for the same alloys under T4 conditions. In general, the impact toughness behavior of aged hypoeutectic alloys depends to a great extent on their aging response at 180 °C (356 °F) or 220 °C (428 °F) aging temperatures. The presence of undissolved intermetallic phases, mainly Al_2Cu and $\alpha-Al_{15}(Mn,Fe)_3Si_2$,

Table 1. (a) AA Standard Chemical Composition of as-Received Alloys,¹³ (b) Actual Chemical Composition of as-Received Alloys

Alloy	Element (wt%)									
	Si	Fe	Cu	Mn	Mg	Ni	Ti	Zn	Sr	B
<i>(a)</i>										
356.1	6.5–7.5	0.50–0.44	0	0.35	0.25–0.45	0	0.1075	0.35	0	0
A413.1	11.0–13.0	1.0	1.0	0.35	0.1	0.50	0.0652	0.50	0	0
Alloy	Element (wt%)									
	Si	Fe	Cu	Mn	Mg	Cr	Ti	B	Sr	Al
<i>(b)</i>										
356	6.3	0.0991	0.0597	<0.0005	0.3143	<0.0005	0.1075	<0.0002	0.0001	93.2
413	11.17	0.3440	0.4875	0.2183	0.0462	0.0240	0.0652	0.0003	<0.0000	87.4

AA Aluminum Association

Table 2. Chemical Composition of the Alloys Used in the Present Study

Alloy code	Element (wt%)									
	Si	Fe	Cu	Mn	Mg	Cr	Ti	B	Sr	Al
<i>356 based alloys</i>										
B*	6.3	0.0991	0.0597	<0.0005	0.3143	<0.0005	0.1075	<0.0002	0.0001	93.2
BDT***	6.29	0.0927	0.0067	<0.0005	0.3171	<0.0005	0.1127	<0.0002	0.0001	93.1
BDS****	6.16	0.0943	0.0032	<0.0005	0.3149	<0.0005	0.1082	<0.0002	0.0159	93.3
BDTS	6.09	0.0925	0.0066	<0.0005	0.3121	<0.0005	0.1122	<0.0002	0.0193	93.3
BDTE**	6.17	0.1781	0.2087	0.0107	0.2854	0.0007	0.3804	0.0360	0.0002	92.6
BDTES	5.96	0.1596	0.1992	0.0101	0.2716	<0.0005	0.4307	0.0360	0.0172	92.8
BDH	6.10	0.0990	0.1124	<0.0005	0.3116	<0.0005	0.1094	<0.0002	0.0002	93.2
BDH4	6.18	0.1052	0.0887	0.0011	0.3102	0.0007	0.1117	<0.0002	0.0001	93.1
<i>413 based alloys</i>										
DC	11.17	0.3440	0.4875	0.2183	0.0462	0.0240	0.0652	0.0003	<0.0000	87.4
CDT	10.98	0.3621	0.4963	0.2465	0.0467	0.0289	0.0701	0.0004	0.0001	87.5
CDS	11.02	0.3583	0.4909	0.2480	0.0428	0.0289	0.0630	<0.0002	0.0187	87.5
CDTS	11.22	0.3733	0.504	0.2469	0.0435	0.0301	0.1240	0.0003	0.0158	87.3
CDTE	10.28	0.3846	0.4820	0.2375	0.0454	0.0302	0.3279	0.0360	<0.0000	88.0
CDTES	10.47	0.3801	0.4734	0.2374	0.0410	0.0302	0.3431	0.0360	0.0124	87.8
CDH†	10.69	0.3561	0.4968	0.2462	0.0487	0.0291	0.0645	0.0002	<0.0000	87.8
CDH4††	10.87	0.3593	0.4972	0.2424	0.0477	0.0295	0.0648	0.0002	0.0001	87.7

Low and high values of grain refiner and Sr levels used in the different alloys are given in bold

* Low grain refining

** High grain refining

*** Low Sr content

**** High Sr content

† 0.25 mL H/100b Al

†† 0.4 mL H/100 g Al

increases alloy brittleness and thus also reduces alloy toughness. The segregation of Al₂Cu caused by Sr addition is a further parameter to be considered. The combination of

Sr modification and solution treatment increases the impact energy values of alloys to a noticeable degree, particularly at low levels of intermetallics. The application of Sr

Table 3. Grain Size of the 356 and 413 Alloys Studied

Alloy code	Ti content	Grain size (μm)	Standard deviation (μm)
B	0.1075	811	37.8
BDT	0.1127	692	29.3
BDTE	0.3804	289	78
C	0.0652	2466	48.6
CDT	0.0701	2156	269
CDTE	0.3279	275	37

modification in conjunction with solution treatment significantly improves both the crack initiation and the crack propagation resistance, and consequently, results in a noticeable improvement in the overall impact energy of the alloys.

The present investigation was undertaken to study the effect of different metallurgical parameters on the microstructure and performance of 356 (Al–Si–Mg) and 413 (Al–Si–Mg–Cu) alloys covering a range of Si content and consequently the response to heat treatment. These alloys are among the alloys that are widely used in the automotive industries. The parameters studied included: alloy composition, hydrogen level, modification by strontium (Sr), grain refining (mainly by TiB_2) as well as heat treatment.

Experimental Procedure

The chemical compositions of the as-received 356 and 413 alloys are given in Table 1b which are very close to those recommended by the Aluminum Association standards (Table 1a). The alloys were melted using an electrical

resistance furnace. The melting temperature was maintained at $730 \pm 5^\circ\text{C}$ (to insure high fluidity of the liquid metal and hence sounder castings); the molten metal was degassed using pure dry argon injected into the molten metal ($0.85 \text{ m}^3/\text{h}$) by means of a rotary graphite impeller.

The degassing time/speed was kept constant at 30 min/150 rpm in order to obtain a lower hydrogen level of $\sim 0.1 \text{ mL}/100 \text{ g}$ in the melt. Measured amounts of Al–10 %Sr and Al–5 wt%Ti–1 wt%B master alloys were added to the molten metal after degassing. Samples for chemical analysis were also extracted simultaneously for each melt/casting produced. The chemical compositions representing the average of three spectrometric analyses for each of the alloys investigated are listed in Table 2 (it should be noted that the Si in 356 alloy is slightly below the recommended level as listed in Table 1a). The melt hydrogen level was increased through addition of raw potatoes to the melt to obtain levels of $0.2 \text{ mL}/100 \text{ g}$ (low) and $0.4 \text{ mL}/100 \text{ g}$ (high) and determined using the Leco subfusion technique.

A star-like mold which provided a high cooling rate was used to prepare the impact and the hardness test specimens as well as to take metallographic measurements. Each casting provides ten impact bars which are cut from the casting and then machined to the required ASTM specifications to conduct Charpy impact tests subsequently. Hardness test specimens measuring $10 \text{ mm} \times 10 \text{ mm} \times 55 \text{ mm}$ were cut from the casting and polished with fine sandpaper to remove any machining marks.

The hardness and impact test samples prepared for each alloy composition were solution heat-treated (SHT) at 540°C (1004°F) for 8 h for the 356 based alloys and at 495°C (923°F) for 8 h for the 413 based alloys, quenched in warm water at 65°C (149°F) and artificially aged for

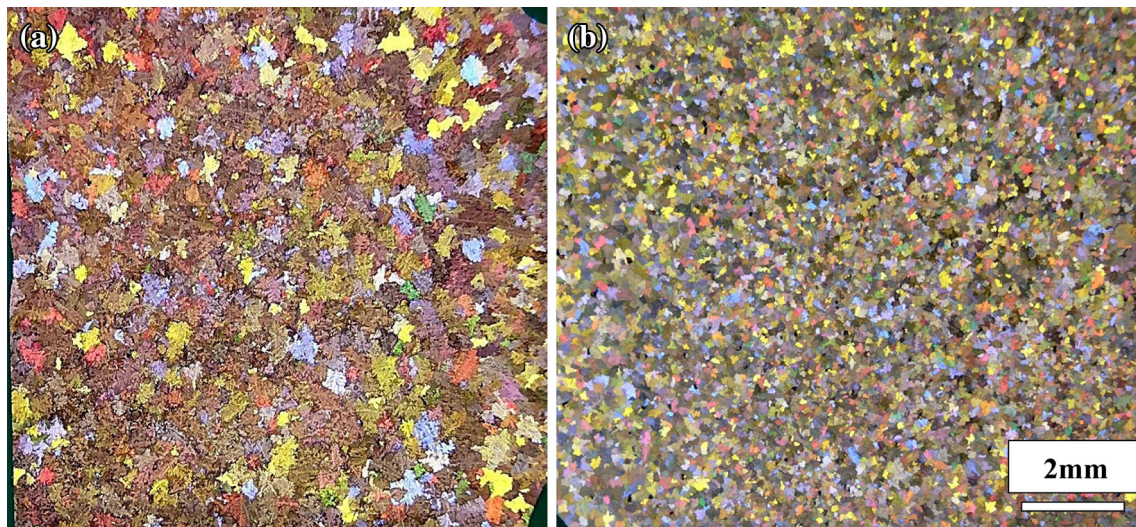


Figure 1. Macrostructure of grains observed in 356 alloys following addition of: (a) 0.0075 wt% Ti (DBDT alloy) and (b) 0.25 wt% Ti (DBDTE alloy).

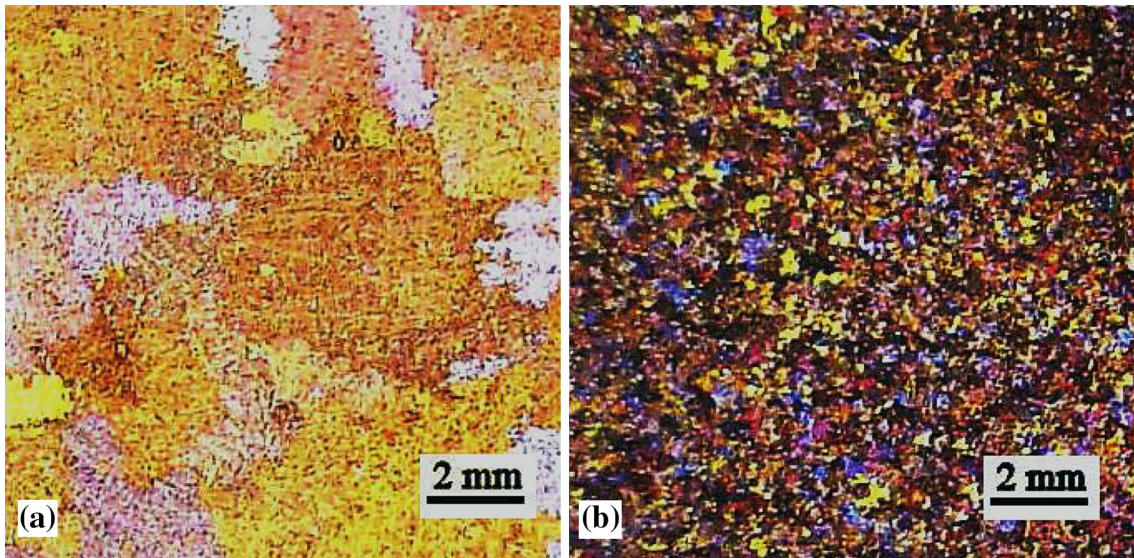


Figure 2. Macrostructure of the grains observed in 413 alloys following the addition of: (a) 0.0075 wt% Ti (DCDT alloy) and (b) 0.25 wt% Ti (DCDTE alloy).

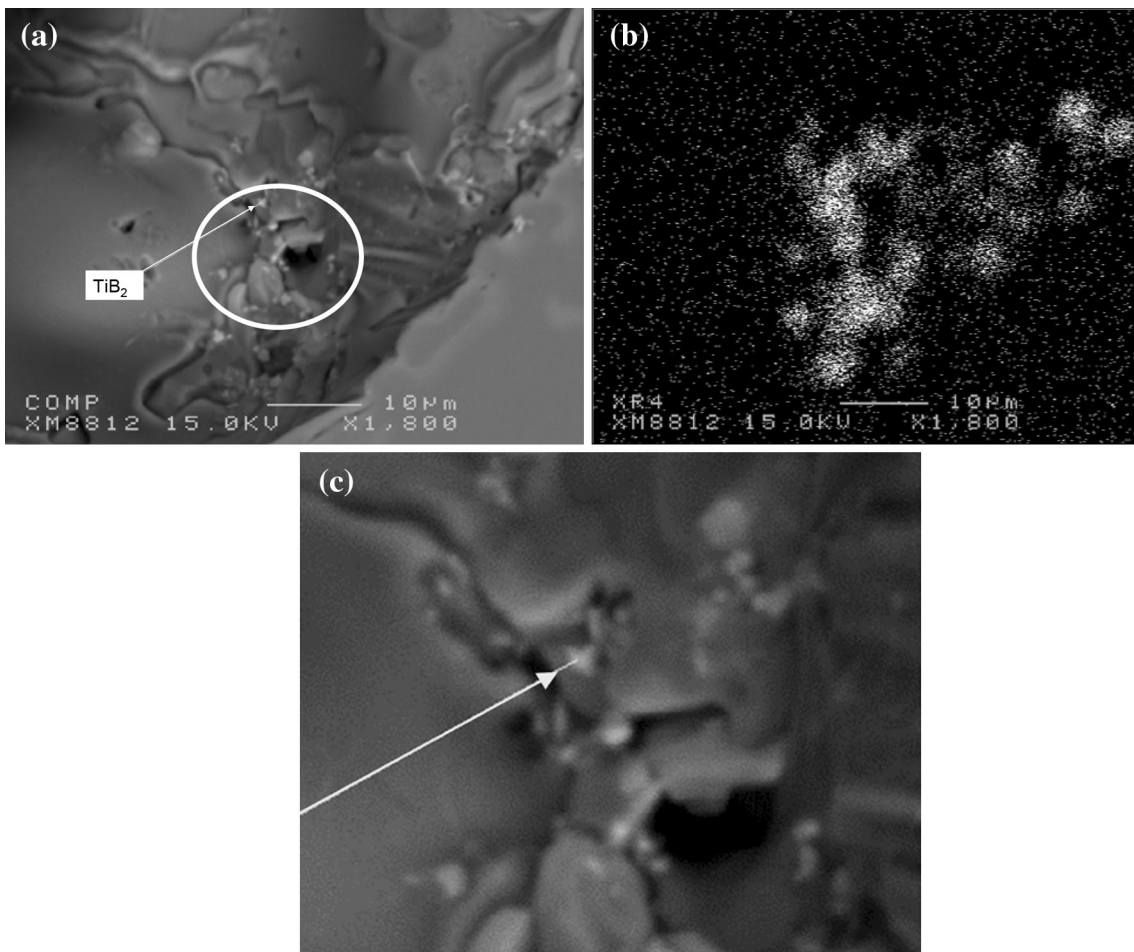


Figure 3. (a) Backscattered electron image showing fine TiB_2 particles in DBDTE alloy and (b) corresponding X-ray image of Ti, (c) an enlarged image of the circled area in (a).

Table 4. Si Particle Characteristics of 356 Alloys (A) Before Solution Heat Treatment, (B) After Solution Heat Treatment

Alloy code	Area (μm^2)		Length (μm)		Roundness (%)		Aspect ratio		Density (particles/ mm^2)
	Average	SD	Average	SD	Average	SD	Average	SD	
<i>(A)</i>									
B	13.05	24.38	7.80	8.93	51.42	29.85	2.95	1.76	6615
BD	13.43	25.06	7.97	9.19	51.28	30.05	3.04	1.82	6081
BDT	26.21	42.42	11.81	13.36	47.13	30.38	3.03	1.80	3902
BDS	5.44	9.44	4.07	3.90	64.62	27.12	2.20	1.05	14,090
BDTS	3.12	6.08	2.90	2.86	71.25	25.11	2.06	0.89	20,921
BDH	12.35	21.07	8.00	9.18	50.50	29.58	3.17	1.94	7697
BDH4	12.95	25.89	7.74	9.37	51.86	29.84	3.12	1.92	5902
BDTE	18.88	38.05	8.44	12.14	57.99	32.72	2.50	1.41	3696
BDTES	3.17	7.98	3.00	5.92	69.65	26.64	2.19	1.03	24,210
<i>(B)</i>									
B	21.74	28.26	9.55	8.95	58.08	27.03	2.84	1.71	3776
BD	18.09	26.28	8.49	8.40	59.67	26.93	2.80	1.64	4203
BDT	28.64	39.19	11.24	10.94	56.40	27.63	2.94	1.81	3291
BDS	11.83	15.68	5.04	4.02	76.44	21.29	1.85	0.84	7256
BDTS	11.36	14.17	4.84	3.80	77.73	20.92	1.78	0.80	6010
BDH	21.70	26.26	9.65	8.90	57.76	26.22	2.91	1.69	4456
BDH4	18.29	24.53	8.84	8.13	57.72	26.37	2.91	1.69	4465
BDTE	27.10	38.44	10.16	10.80	60.71	29.32	2.62	1.56	3041
BDTES	9.02	11.62	4.18	4.81	80.77	18.55	1.71	0.78	9782

5 h at 155, 180, 200, 220 (311, 356, 392, 428 °F) and 240 °C (464 °F). All heat treatments were conducted in a forced-air Blue M electric furnace equipped with a programmable temperature controller, accurate to ± 2 °C. For each individual heat treatment condition, five test bars were used.

The hardness measurements were carried out on the as-cast and heat-treated samples using a Brinell hardness tester, applying a steel ball of 10 mm diameter and a load of 500 kgf for 30 s. An average of four readings obtained from two perpendicular surfaces was taken to represent the hardness value in each case.

A computer-aided instrumented SATEC SI-1 Universal Impact Testing Machine (SATEC Systems Inc., Model SI-1D3) was used to carry out the impact tests. A data acquisition system connected to the impact machine monitored the dynamic behavior of the test specimen and measured the load and energy values as a function of time. Samples for metallographic observations were sectioned from the impact-tested bars of all the alloys studied about ~ 10 mm below the fracture surface. The samples were mounted in bakelite and polished to a fine finish.

The microstructures of the polished sample surfaces were examined using an optical microscope linked to a Clemex image analysis system. The eutectic silicon particle characteristics, including area, length, aspect ratio, roundness and density, were measured and quantified. For each sample, 50 fields at a magnification of $500\times$ were examined, so as to cover the entire sample surface in a regular and systematic manner. In addition, porosity measurements were carried out, over 50 fields per sample, at a magnification of $100\times$. The porosity parameters measured were percentage porosity, pore area and pore length. As a rule, the outer edges of a sample were avoided in taking these measurements so as to eliminate any distortions which might occur in the peripheral regions. Some selected samples were examined using a Hitachi SU-8000 field emission gun scanning electron microscope (FESEM). Prior to examination, samples were re-polished using ion bombardment to remove the surface oxides.

For measurements of grain size, the polished samples were chemically etched using Keller's reagent (66 vol% HNO_3 , 33 vol% HCl and 1 vol% HF) and diluted with water to slow down the etching process. Once etching was

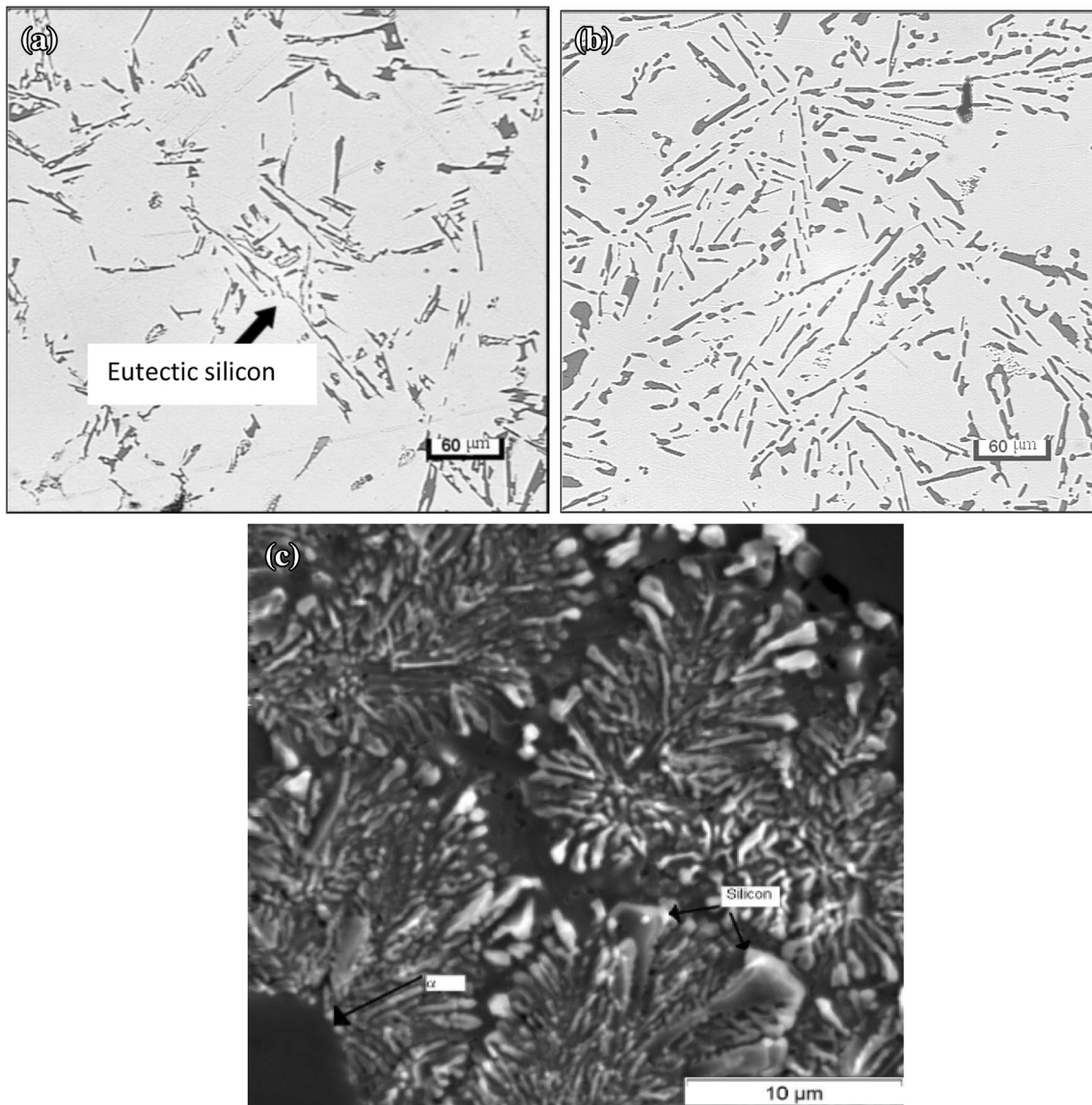


Figure 4. Changes in the morphology of non-modified eutectic Si particles in BDT alloy: (a) as-cast, (b) after solution heat treatment, (c) extracted eutectic Si particles in as-cast 356 alloys.¹⁵

completed, the sample surfaces were rinsed, dried and then photographed using a setup consisting of four projectors emitting red, blue, green and yellow light. The grain sizes were measured from the digital photographs using Sigma Scan Pro 4.0 software, employing a method similar to the line intercept method. The grain size for each sample was obtained as the average of 80 readings.

Results and Discussion

Microstructural Characterization

It is a well-established fact that grain size in Al–Si alloys is greatly influenced by the added amount of TiB₂.^{11,12} Sigworth and Guzowski¹⁴ used Al–5 %Ti–1 %B master

alloy to obtain minimum grain size in 356 alloys. In the present study, three concentrations of TiB₂ were used, corresponding to 0, 0.0075 and 0.25 wt% Ti. The grain sizes obtained are listed in Table 3. Using low concentration of TiB₂, i.e., 0.0075 % Ti, a slight decrease in the grain size was observed (from 811 to 692 μm for 356 alloys and from 2466 to 2156 μm for 413 alloys). Increasing the TiB₂ concentration—measured by the amount of Ti—to 0.25 % reduced the grain size to 289 μm for 356 alloys and to 275 μm for 413 alloys (approximately 90 %) as shown in Figure 1. Figure 2 shows the grain size in CDTE alloy grain refined with 0.25 % Ti, whereas Figure 3 shows the size and distribution of TiB₂ particles as viewed within a small pore using the FESEM technique. The average TiB₂ particle size is about 300–500 nm.

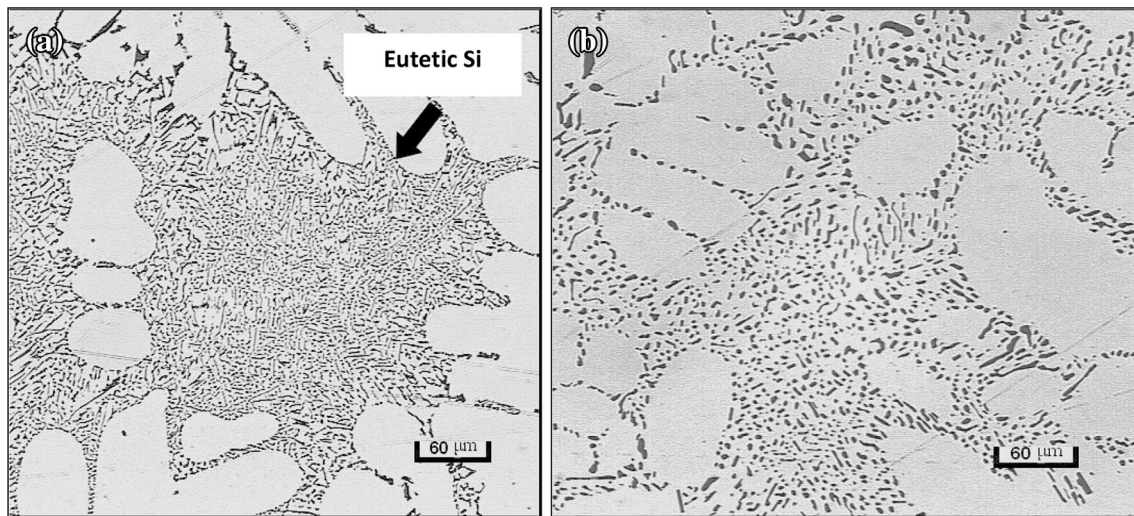


Figure 5. Morphology of eutectic Si in Sr-modified 356 (BDS) alloy: (a) as-cast, (b) after solution heat treatment.

Table 5. Si Particle Characteristics of 413 Alloys (A) Before Solution Heat Treatment, (B) After Solution Heat Treatment

Alloy code	Area (μm^2)		Length (μm)		Roundness (%)		Aspect ratio		Density (particles/ mm^2)
	Average	SD	Average	SD	Average	SD	Average	SD	
(A)									
C	21.32	45.04	10.61	14.85	49.28	31.74	3.48	2.17	5226
CD	28.15	48.75	11.81	14.74	51.11	31.92	3.03	1.90	4345
CDT	26.98	48.06	12.45	16.42	51.97	33.34	3.19	2.20	4334
CDS	2.24	2.52	2.40	1.77	78.05	20.87	1.87	0.73	67,493
CDTS	2.75	2.82	2.63	1.84	76.55	21.55	1.85	0.69	75,149
CDH	20.13	38.17	10.35	13.74	51.34	32.42	3.19	2.01	5500
CDH4	35.84	60.12	14.25	17.97	49.02	32.14	3.23	2.05	3091
CDTE	32.62	53.26	12.87	15.16	50.94	32.74	2.97	1.76	3394
CDTES	1.69	5.64	2.07	6.29	79.20	20.69	1.90	0.74	74,668
(B)									
C	33.56	50.01	14.17	15.16	47.92	30.04	3.53	2.18	3504
CD	21.17	30.82	11.13	11.25	48.87	28.13	3.48	2.01	5751
CDT	33.16	51.36	13.61	15.11	50.08	30.19	3.30	2.08	3442
CDS	3.79	3.80	2.90	2.03	82.21	17.53	1.69	0.65	31,343
CDTS	3.08	2.94	2.58	1.61	83.95	15.37	1.67	0.60	39,908
CDH	21.62	35.20	11.18	12.16	48.18	28.32	3.59	2.14	5298
CDH4	31.14	51.11	13.27	15.42	49.16	29.64	3.48	2.10	3754
CDTE	31.54	52.1	11.69	14.10	57.09	31.51	2.81	1.68	3672
CDTES	3.21	5.71	2.62	5.80	81.70	17.51	1.76	0.69	29,180

Table 4 lists the measured parameters of eutectic Si particles in 356 alloys before and after solution heat treatment. As may be seen, the average area of the Si particles of non-modified alloys exhibits an increase after solution heat

treatment. Considering the Sr-modified alloys, the Si particles revealed a tendency for spheroidization followed by coarsening. The changes in the morphology of the Si particles from acicular to fibrous explain the observed

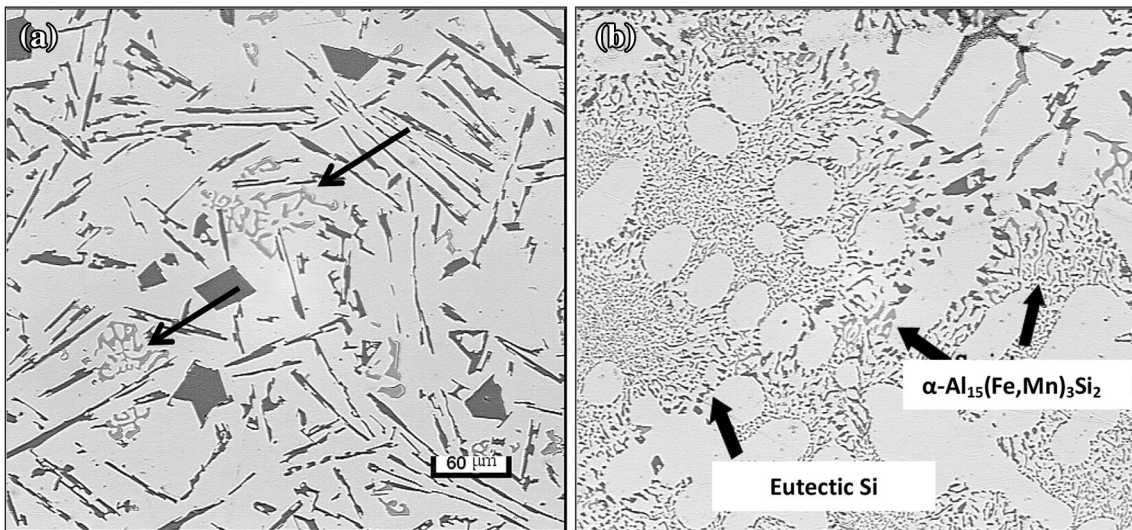


Figure 6. Eutectic Si particle distribution in 413 alloy: (a) before Sr modification-CDT alloy note the precipitation of α -Fe in the interdendritic regions, (b) after Sr modification-DCDS alloy note the precipitation of α -Fe within the α -Al.

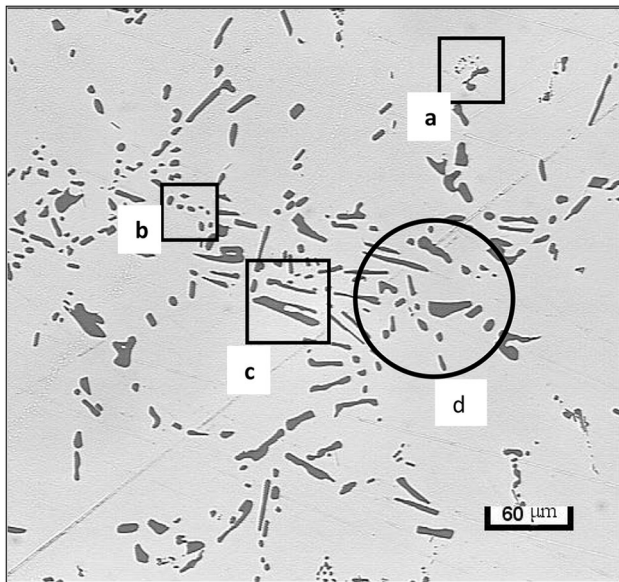


Figure 7. Eutectic Si particles in DC alloy following prolonged solutionizing at 495 °C: (a) dissolution of fine Si particles, (b) fragmentation, (c, d) coarsening.

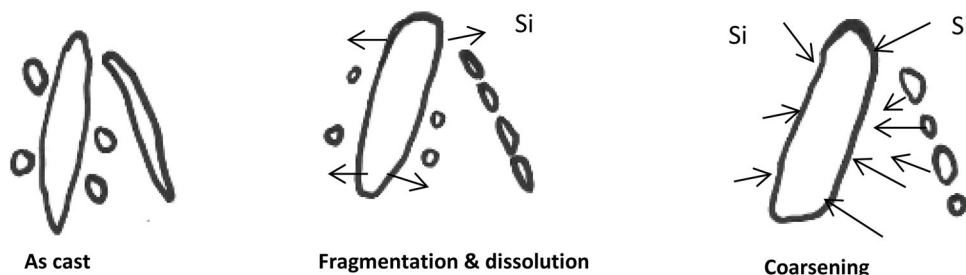


Figure 8. Proposed schematic diagram for the observed increase in the particle size after solution heat treatment.

variation in Si particle measurements as exemplified in Figure 4. Figure 5a shows typical Sr-modified alloys revealing ultra-fine Si particles compared to Figure 4a. Following solution heat treatment at 540 °C (1004 °F) for 8 h, the Si particles underwent spheroidization and coarsening as displayed in Figure 5b. Figure 4c is an example of Si particles observed in non-modified 356 alloy in the as-cast condition revealing a significant variation in their size across the sample surface,¹⁵ explaining the large standard deviations reported in Table 4.

Table 5 lists the measured Si particle parameters for 413 alloys before and after solution heat treatment. As in the case of 356 alloys, non-modified alloys revealed a slight increase in the particle size after solution heat treatment. However, the addition of Sr resulted in more or less uniform distribution of fibrous Si particles with spheroidization after solution heat treatment. The presence of trace elements in 413 alloy (mainly Fe, Cr and Mn) resulted in the precipitation of α -Al₁₅(Fe,Mn,Cr)₃Si₂, as shown in Figure 6. In order to arrive at a clear understanding of the

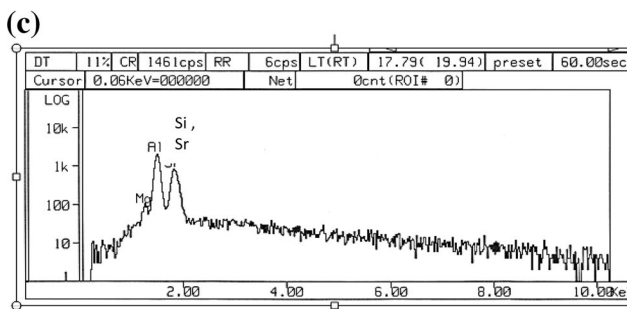
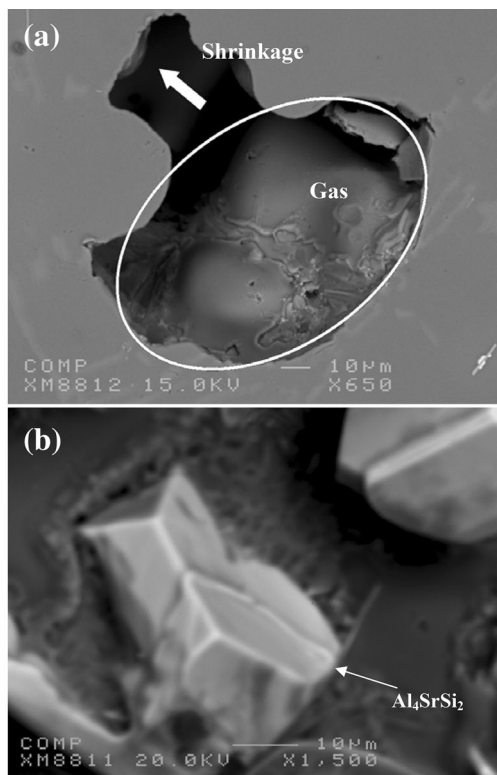


Figure 9. (a) A mixture of gas and shrinkage porosity observed in CDH4 alloy, (b) presence of Al_4Si_2Sr particles in DCDTES alloy in the as-cast condition, (c) EDS corresponding to (b). $Si K_{\beta} = 1.84 \text{ keV}$, $Sr L_{\alpha} = 1.94 \text{ keV}$.

observed increase in the Si particle size in non-modified alloys, the solutionizing time was increased to 48 h (413 alloys). Figure 7 exemplifies the increase in the Si particle thickness following prolonged solutionizing treatment (SHT) at 495 °C (923 °F)—circled area—compared to Figure 6a. Figure 8 shows a schematic representation of the proposed mechanism of coarsening phenomenon based on the theory developed by Ostwald.¹⁶

Different types of porosity have been reported in the present study. They include gas porosity caused by the increase in the hydrogen content, shrinkage porosity due to poor feeding, a mixture of gas and shrinkage porosity (Figure 9a), oxide films or a mixture of these types.^{17–19} Table 6 lists the measured porosity parameters in 413 alloys. In addition to the porosity caused by increasing the hydrogen content (DCDH4 alloy vs. DC alloy), addition of Sr also leads to porosity formation as given in Table 6 for 413 alloys (DCDTES alloy vs. DC alloy). Obviously, the increase in the porosity due to hydrogen addition is an order of magnitude higher than that introduced by increasing the amount of added Sr. Also, over-modification appeared in the precipitation of Al_4SrSi_2 in the form of tetrahedral particles as displayed in Figure 9b.²⁰

Hardness and Impact Properties

The following aging sequence of an Al–Mg–Si alloy is generally accepted as being correct:²⁰ $\alpha \rightarrow \text{G.P. zone} \rightarrow \text{metastable } \beta' \text{ phase} \rightarrow \text{equilibrium } \beta'' \text{ phase}$. The β'' phase is considered to be extremely important because it may play a major role as an effective strengthening precipitate in the Al–Mg–Si alloys.²¹ The chemical composition of the β'' phase is Si:Al:Mg = 6:3:1. In a recent study²² it was proposed that the precipitation sequence was: clusters of Si atoms \rightarrow GP-I zones \rightarrow GP-II zones/ $\beta'' \rightarrow \beta' \rightarrow \beta\text{-Mg}_2\text{Si}$. Ohmori et al.²³ studied the aging process in Al–Si–Mg alloys during continuous heating. Their results show a slight hardening at temperatures

Table 6. Porosity Characteristics Observed in the 413 Alloys

Alloy code	Area (μm^2)		Length (μm)		Aspect ratio		Density (pores/ mm^2)
	Average	SD	Average	SD	Average	SD	
C	157.1	244.9	15.10	8.226	1.34	0.38	0.17
CD	82.29	71.44	14.79	9.074	2.12	0.92	0.19
CDT	454.8	4622	29.66	24.81	1.76	0.65	0.83
CDS	832	2369	30.31	46.70	1.76	0.65	2.19
CDTS	934.9	2962	31.57	61.09	1.87	0.80	1.14
CDH	149.3	341.1	16.70	21.54	1.71	0.63	1.72
CDH4	2840	10,241	45.91	81.66	1.69	0.61	2.08
CDTE	185.8	4825	14.90	19.39	1.67	0.75	5.97
CDTES	865.1	4415	30.45	35.30	1.70	0.66	6.58

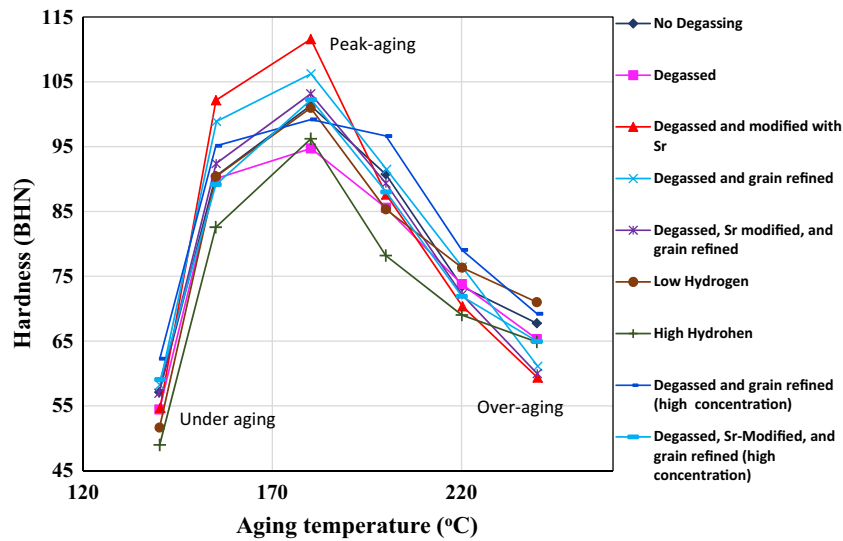


Figure 10. Variation in the hardness of 356 alloys as a function of aging temperature.

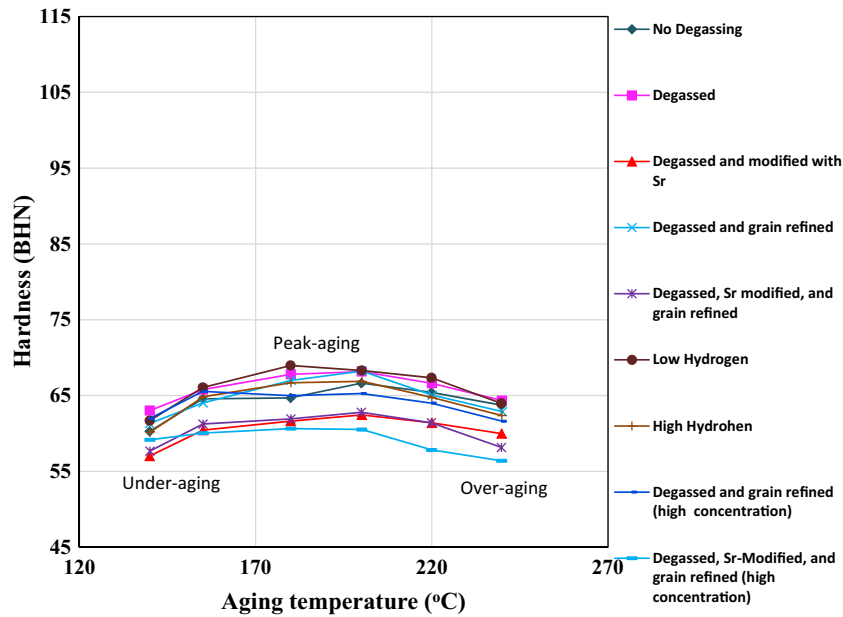


Figure 11. Variation in the hardness of 413 alloys as a function of aging temperature.

77–152 °C (171–306 °F) caused by the formation of solute atom clusters, a small amount of softening at temperatures around 177 °C (351 °F), and a sharp and large hardening at around 277 °C (531 °F), attributed to the precipitation of needle-shaped β'' , followed subsequently by a large drop in hardness due to the formation of β -Mg₂Si.

Figure 10 represents the hardness data for the 356 alloys used in the present study following aging at different temperatures. Apparently the variation in the metallurgical parameters has a minor effect on the alloy strength. However, varying the aging temperatures resulted in a noticeable

change in the alloy hardness due to precipitation of Mg₂Si phase particles.²⁴ In contrast to the work of Ohmori et al.,²² only a single peak was observed at 180 °C (356 °F), caused by the precipitation of both β' and β'' particles, followed by continuous softening due to progress in the precipitation and coarsening of incoherent β -Mg₂Si.²⁵

Tash et al.²⁶ and Moustafa et al.²⁷ found that the 319 alloy hardness first increased with an increase in aging temperature up to 180 °C (356 °F) and thereafter decreased as the aging temperature was increased. The increase in hardness with the addition of Cu and Mg may be attributed to the

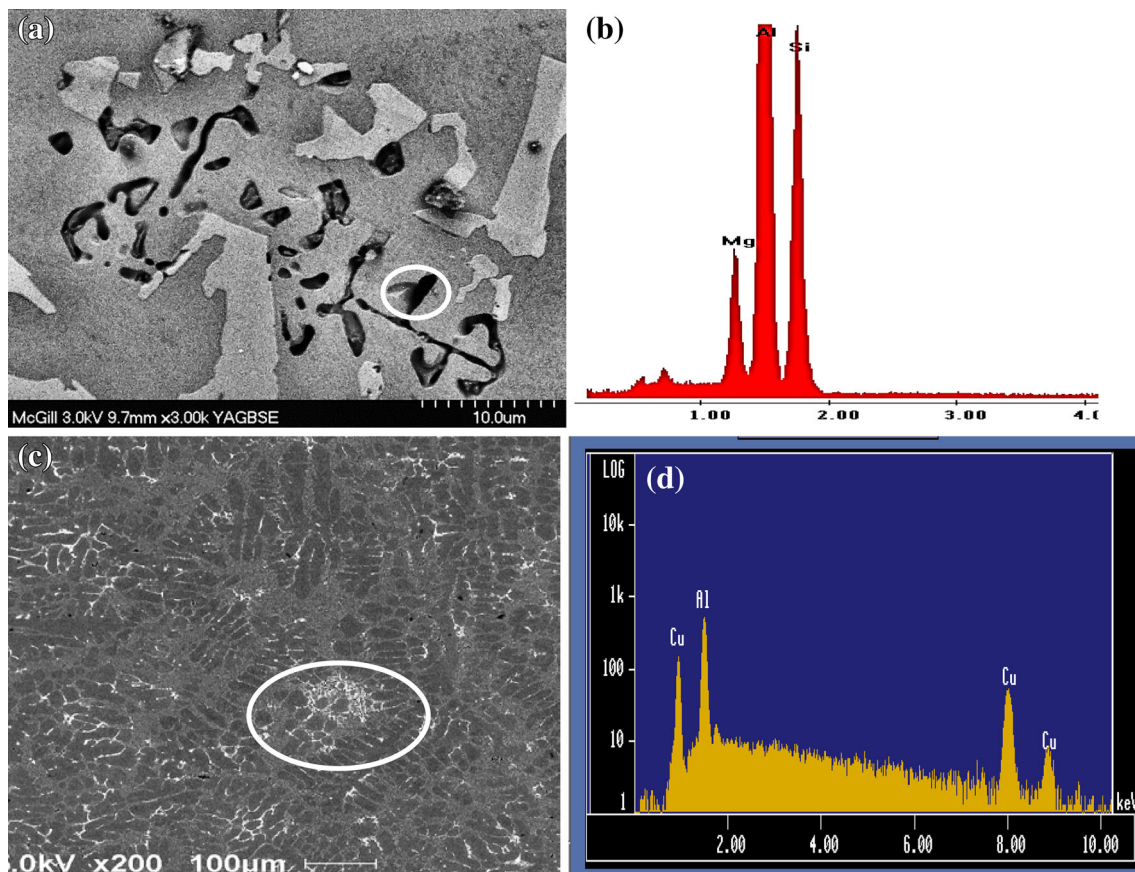


Figure 12. Electron images of 356 and 413 alloys in the as-cast condition: (a) backscattered-356 alloy, (b) EDS spectrum corresponding to the white circle in (a) showing peaks of Si and Mg, (c) backscattered-413 alloy, (d) EDS spectrum corresponding to the white circle in (c) showing peaks of Al and Cu.

formation of the hard and brittle (metastable) intermetallic Al_2Cu and Al_2CuMg phases, as well as to an increased bonding of the Si particles with the matrix, where the thermal energy is sufficient to precipitate such intermediate phases. The decrease in hardness at aging temperatures above $180\text{ }^\circ\text{C}$ ($356\text{ }^\circ\text{F}$) may be due to the coarsening of the various microconstituents as well as to a decrease in cohesion with the matrix.

The coarsening of hard intermetallic phases may reduce the barrier to dislocation movement and, hence, to flow stress/hardness. Silicon alone contributes little to the strength of aluminum casting alloys, yet provides an observably effective level of strengthening when combined with magnesium to form Mg_2Si . The Mg_2Si phase is soluble in the alloy to a limit of $\sim 0.7\text{ wt}\%$ Mg and provides the precipitation-strengthening basis for the heat-treatable alloys.²⁸

Figure 11 displays the variation in the hardness of 413 alloys as a function of aging temperature. As in the case of 356 alloys, variation in the metallurgical parameters has a slight effect on the alloy strength. However, the maximum

attainable strength at $180\text{ }^\circ\text{C}$ ($356\text{ }^\circ\text{F}$) is about 67 BHN compared to 115 BHN in the case of 356 alloy (DBDTES alloy, degassed, Sr-modified and grain refined with 0.25 wt% Ti). It should be kept in mind that the 413 alloys contain very low amount of Mg, approximately 0.04 %, compared to 0.3 % in the case of 356 alloys. Thus, hardening by Mg_2Si phase particles is more effective than hardening by Al_2Cu phase precipitation which is in good agreement with the published literature.²⁹ Figure 12 shows the difference in the microstructure of the two alloys used in the present work, whereas Figure 13 depicts the morphology and size of the precipitates observed in 356 and 413 alloys aged at $180\text{ }^\circ\text{C}$ for 5 h.

Paray et al.³⁰ reported that Sr modification improved the unnotched impact strength of both as-cast and heat-treated A356.0 and 413.0 alloys. Once the initial modification is made, there is a good retention of mechanical properties.³¹ The work of Li et al.³² showed that the addition of both Mg and Sr can lead to severe segregation of the Al_2Cu phase in 319.2 alloys, resulting in the production of large amounts of the coarse block-like phase, compared to the finer eutectic-like form. These segregated block-like Cu-rich

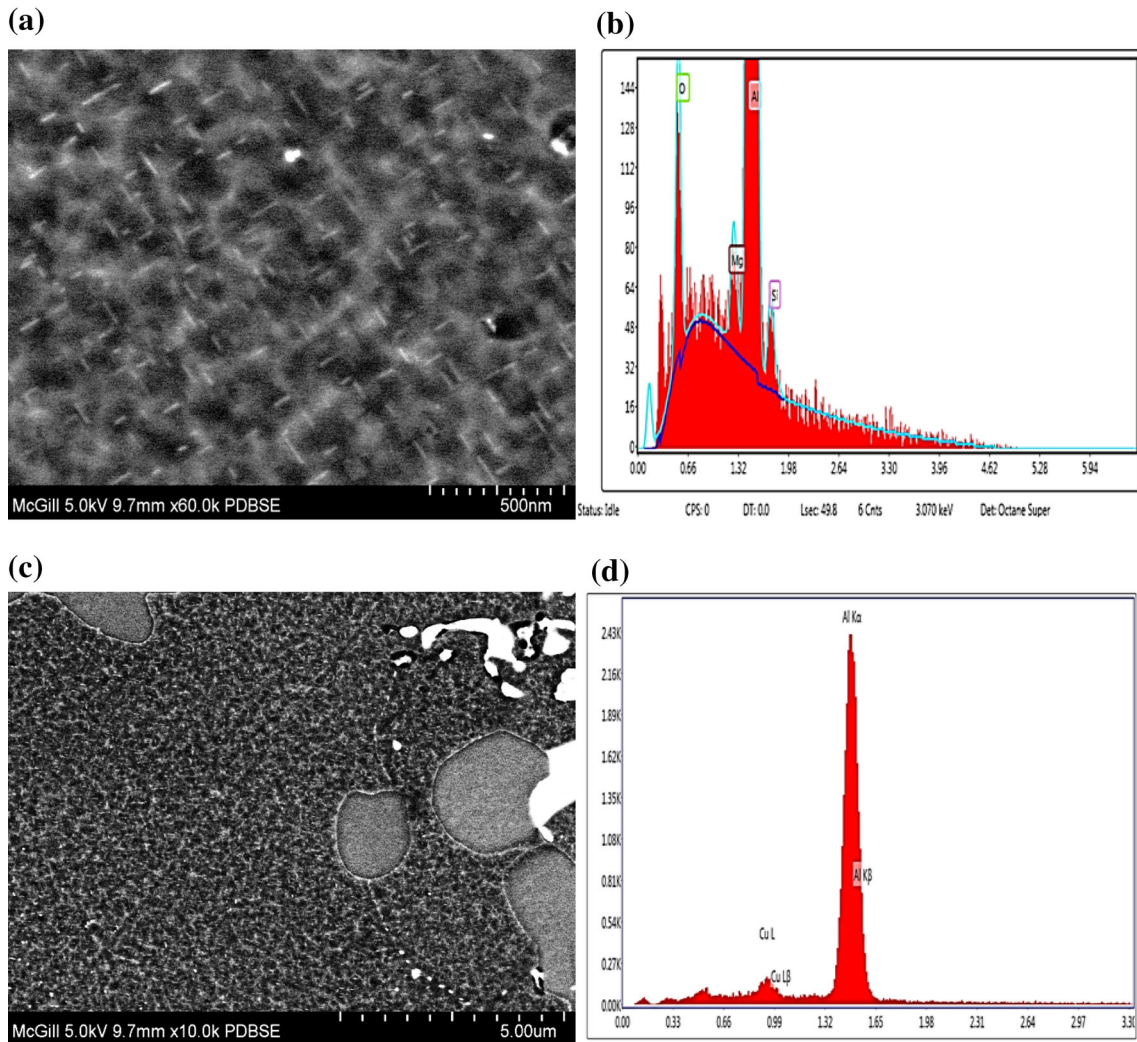


Figure 13. Precipitation observed in alloys aged at 180 °C: (a) Mg_2Si in BDS (356) alloy, (b) EDS spectrum corresponding to (a), (c) Al_2Cu in CDS (413) alloy, (d) EDS spectrum corresponding to (c).

phase particles decrease the impact strength of the Al–Si–Cu–Mg alloys.³³

Figure 14a reflects the importance of the applied metallurgical parameters on the performance of 356 alloys. In principle, all modified alloys exhibited better impact energies compared to those only grain refined. The presence of porosity in Sr-modified alloys lead to lower hardness in comparison with grain-refined alloys. Best impact results were obtained when the alloy was degassed, grain refined and properly modified. Increasing the hydrogen content and hence the porosity volume fraction resulted in toughness energy values as low as 5 J. Similar observations were

noted for the 413 alloys as shown in Figure 14a where most of the Sr-modified alloys exhibited high impact energies coupled with low strength. The scattering in the results is mainly due to the presence of porosity or oxide films.³⁴

It is quite useful to examine the fracture profile on sections perpendicular to the fracture surface. This can be carried out using an optical microscope. In this way, the origin of the fracture can be examined to determine if important microstructural abnormalities are present that either caused or contributed to fracture initiation. It is also possible to determine if the fracture path at the initiation site is transgranular or intergranular and to determine whether the

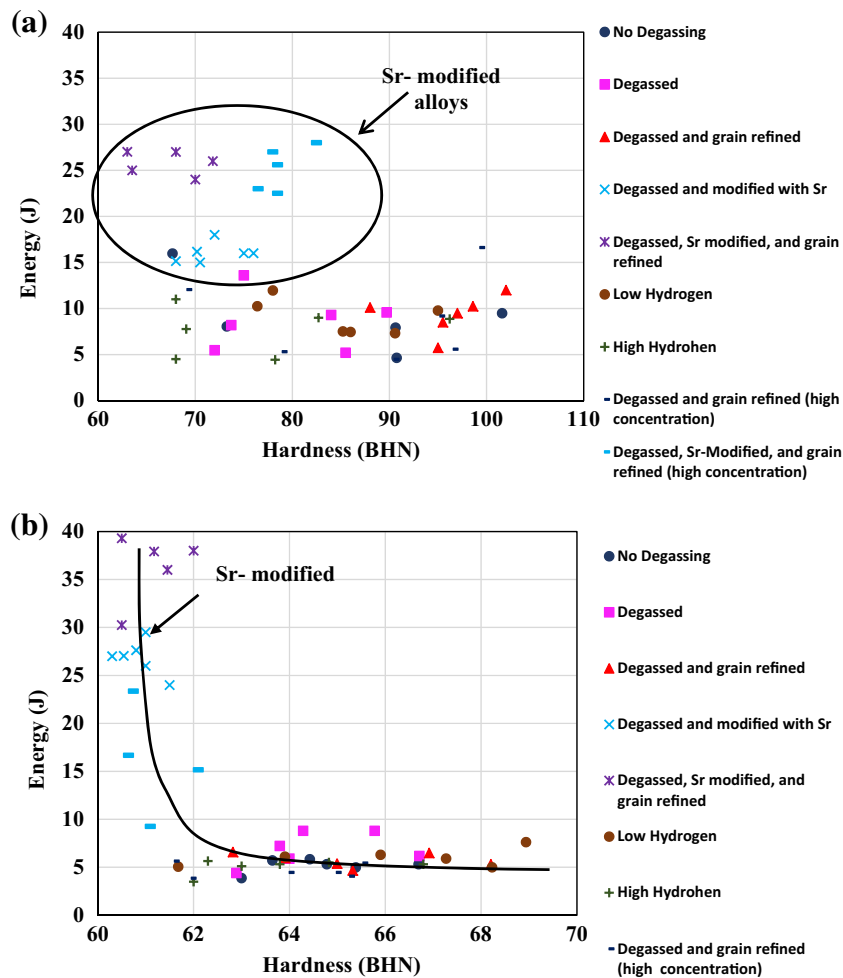


Figure 14. (a) Hardness–impact energy relationships in 356 alloys. (b) Hardness–impact energy relationships in 413 alloys.

fracture path is specific to any phase or constituent present. Some examples of the longitudinal sections of the 413 alloy samples are presented in this section with a view further clarifying the fracture process in these samples.

The optical micrograph presented in Figure 15a shows the polished longitudinal section of the fractured non-modified CD alloy following solution heat treatment, revealing how crack initiation occurs by the cleavage and/or the transgranular fracture of the Si particles. A higher-magnification micrograph, Figure 15b, of the fracture surface corresponding to the arrowed area in (a), shows how the crack propagates further along the fracture surface by cleavage of coarse Si particles. Compared to the micrographs shown in Figure 15a, b, those of Figure 15c, d were obtained from the 413 alloy sample coded CDTES (degassed, Sr-modified and grain refined) corresponding to high energy conditions. Due to the relatively large volume fraction of elastic Al in the matrix, the tips of the dendrites are more rounded than sharp (Figure 15c, arrowed). In this case, the crack propagates through the less ductile Al–Si regions (Figure 15d, arrowed).

Conclusions

Based on the results documented in the present study, the following conclusions may be drawn:

1. Increasing the amount of introduced TiB_2 (measured by increasing the amount of Ti) from 0.0075 to 0.25 wt% reduces the alloy grain size by about 90 %.
2. In Sr-modified 413 alloys, the $\alpha-Al_{15}(Fe,Mn,Cr)_3Si_2$ intermetallic phase precipitates prior to precipitation of $\alpha-Al$.
3. A new mechanism based on Ostwald theory was proposed to explain the coarsening in eutectic Si particles in non-modified alloys during solutionizing treatment.
4. Changing the metallurgical parameters (hydrogen content, TiB_2 concentration, Sr concentration) has no significant effect on the alloy hardness with respect to the precipitation taking place during aging.

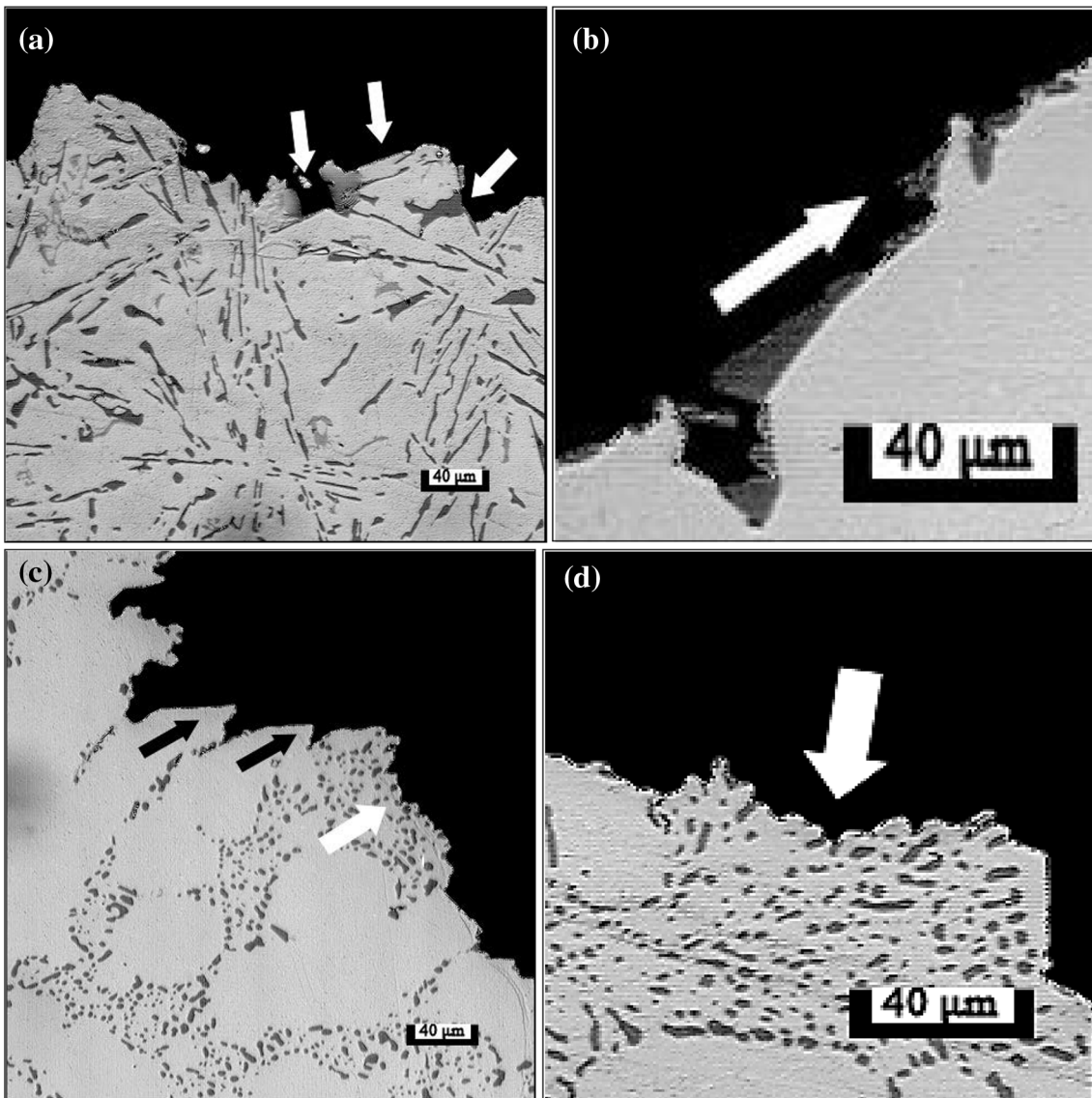


Figure 15. Microstructures beneath the fracture surface in 413 alloys following solution heat treatment: (a) non-modified CD alloy, low-magnification, (b) high-magnification micrograph of (a), (c) Sr-modified CDTES alloy, low-magnification, (d) high-magnification micrograph of (c).

5. Hardening by Al_2Cu precipitation (413 alloys) is much less compared to the hardening achieved by Mg_2Si (356 alloys).
6. In contrast to hardness, impact energy is found to be sensitive to variations in the applied metallurgical parameters. Best results are obtained for degassed, Sr-modified and grain-refined alloys. Due to porosity formation associated with Sr addition, some scatter in the values is noted.
7. Modifying the 413 alloys with 200 ppm Sr results in a more even distribution of the spheroidized eutectic Si particles and hence improves the alloy toughness.

Acknowledgments

The authors would like to thank Ms Amal Samuel for enhancing the quality of art work in the present article.

REFERENCES

1. T. Kobayashi, *Strength and Toughness of Materials* (Agne Gijutsu Center, Springer, Tokyo, 2004)
2. M.A. Meyers, K.K. Chawla, *Mechanical Behavior of Materials*, 2nd edn. (Cambridge University Press, New York, 2009)

3. Metals Handbook, *Mechanical Testing and Evaluation*, vol. 8, 10th edn. (American Society of Metals, Metals Park, 2000), pp. 596–611
4. J.F. Shackelford, *Introduction to Materials Science for Engineering*, 2nd edn. (Macmillan, New York, 1988), pp. 325–332
5. V.A. Mosneaga, T. Mizutani, T. Kobayashi, H. Toda, Impact toughness of weldments in Al–Mg–Si alloys. *Mater. Trans.* **43**, 1381–1389 (2002)
6. M.F. Ibrahim, S.A. Alkahtani, K.A. Abuhasel, F.H. Samuel, Effect of intermetallics on the microstructure and tensile properties of aluminum based alloys: role of Sr, Mg and Be addition. *Mater. Des.* **86**, 30–40 (2015)
7. O. Elsebaie, A.M. Samuel, F.H. Samuel, H.W. Doty, Impact toughness of Al–Si–Cu–Mg–Fe cast alloys: effects of minor additives and aging conditions. *Mater. Des.* **60**, 496–509 (2014)
8. D. Casari, A. Fortini, M. Merlin, *Fracture Behaviour of Grain Refined A356 Cast Aluminium Alloy: Tensile and Charpy Impact Specimens* (Convegno Nazionale IGF XXII, Roma, 2013), pp. 314–321
9. O. Elsebaie, A.M. Samuel, F.H. Samuel, H.W. Doty, The effects of mischmetal, cooling rate and heat treatment on the hardness of A319.1, A356.2 and A413.1 Al–Si casting alloys. *Mater. Sci. Eng. A* **486**(1–2), 241–252 (2008)
10. O. Elsebaie, A.M.A. Mohamed, A.M. Samuel, F.H. Samuel, A.M.A. Al-Ahmari, The role of alloying additives and aging treatment on the impact behavior of 319 cast alloy. *Mater. Des.* **32**(6), 3205–3220 (2011)
11. S.K. Shaha, F. Czerwinski, W. Kasprzak, J. Friedman, D.L. Chen, Microstructure and mechanical properties of Al–Si cast alloy with additions of Zr–V–Ti. *Mater. Des.* **83**, 801–812 (2015)
12. E. Samuel, B. Golbahar, A.M. Samuel, H.W. Doty, S. Valtierra, F.H. Samuel, Effect of grain refiner on the tensile and impact properties of Al–Si–Mg cast alloys. *Mater. Des.* **56**, 468–479 (2014)
13. S.L. Bäckerud, G. Chai, J. Tamminen, *Solidification Characteristics of Aluminum Alloys*, vol. 2 (AFS/Skanaluminium, Oslo, 1990)
14. G.K. Sigworth, M.M. Guzowski, Grain refining of hypoeutectic Al–Si alloys. *AFS Trans.* **93**, 907–912 (1985)
15. B.A. Dewhirst, *M.Sc. Thesis* (Worcester Polytechnic Institute, Materials Science and Engineering, USA, 2005)
16. W. Ostwald, *Lehrbuch der Allgemeinen Chemie*, vol. 2, part 1 (Leipzig, 1896)
17. H.R. Ammar, A.M. Samuel, F.H. Samuel, Effects of surface porosity on the fatigue strength of AE425 and PM390 hypereutectic Al–Si casting alloys at medium and elevated temperatures. *Mater. Sci. Eng. A* **473**(1–2), 58–64 (2008)
18. M.G. Kalhapure, P.M. Dighe, Impact of silicon content on mechanical properties of aluminum alloys. *Int. J. Sci. Res.* **4**, 38–40 (2015)
19. C.M. Dinnis, M.O. Otte, A.K. Dahle, J.A. Taylor, The influence of strontium on porosity formation in Al–Si alloys. *Metall. Mater. Trans. A* **35A**, 3531–3541 (2004)
20. E. Samuel, A.M. Samuel, H.W. Doty, S. Valtierra, F.H. Samuel, Intermetallic phases in Al–Si based cast alloys: new perspective. *Int. J. Cast Met. Res.* **27**(2), 107–114 (2014)
21. K. Matsuda, T. Naoi, K. Fujii, Y. Uetani, T. Sato, A. Kamio, S. Ikeno, Crystal structure of the β'' phase in an Al–1.0 %Mg₂Si–0.4 %Si alloy. *Mater. Sci. Eng. A* **262**, 232–237 (1999)
22. L. Hey, H. Zhang, J. Cui, Effects of pre-ageing treatment on subsequent artificial ageing characteristics of an Al–1.01Mg–0.68Si–1.78Cu alloy. *Mater. Sci. Technol.* **26**, 141–145 (2010)
23. Y. Ohmori, L.C. Doan, K. Nakai, Aging process in Al–Mg–Si alloys during continuous heating. *Mater. Trans.* **43**, 246–255 (2002)
24. M.F. Ibrahim, S.A. Alkahtani, F.H. Samuel, Optimizing the Heat Treatment of High Strength Al–Si–Mg and Al–Cu–Mg–Zn Aluminum Alloys for Industrial Applications (Lambert Academic Publishing, 2015)
25. M.F. Ibrahim, S.A. Alkahtani, K.A. Abuhasel, F.H. Samuel, Microstructural Characterization of Beryllium Treated Al–Si Alloys. *Adv. Mater. Sci. Eng.* **2015**, Art. ID 673025, 10 pages (2015)
26. M. Mohandass, A. Venkatesan, S. Karthikeyan, P.S. Prasanth, S.K. Vinuvarshith, Effect of cooling rate on mechanical behaviour of bulk cast of A380 aluminium alloy. *Int. J. Eng. Technol.* **6**, 374–380 (2014)
27. D. Apelian, *Aluminum Cast Alloys: Enabling Tools for Improved Performance. Worldwide Report* (NADCA, Wheeling, 2009), p. 59
28. A.M.A. Mohamed, F.H. Samuel, S.A. Alkahtani, Microstructure, tensile properties and fracture behavior of high temperature Al–Si–Mg–Cu cast alloys. *Mater. Sci. Eng. A* **577**, 64–72 (2013)
29. F. Paray, J.E. Gruzleski, Microstructure–mechanical property relationships in a 356 alloy, part 1: microstructure. *Cast Metals* **7**(1), 29–40 (1994)
30. A.M. Samuel, G.H. Garza-Elizondo, H.W. Doty, F.H. Samuel, Role of modification and melt thermal treatment processes on the microstructure and tensile properties of Al–Si alloys. *Mater. Des.* **80**, 99–108 (2015)
31. Z. Li, A.M. Samuel, F.H. Samuel, C. Ravindran, S. Valtierra, H.W. Doty, Einflussfaktoren auf die Auflösung der CuAl₂-phase in der Legierung 319. *Giesserei-Praxis* **3**, 99–108 (2004)
32. S.A. Kori, M.S. Prabhudev, T.M. Chandrashekharaia, Studies on the microstructure and mechanical properties of A356 alloy with minor additions of copper and magnesium. *Trans. Indian Inst. Met.* **62**, 353–356 (2009)
33. K.A. Abuhasel, M.F. Ibrahim, E.M. Elgallad, F.H. Samuel, On the impact toughness of Al–Si cast alloys. *Mater. Des.* **91**, 388–397 (2016)
34. G. Zhang, J. Zhang, B. Li, C. Wei, Characterization of tensile fracture in heavily alloyed Al–Si piston alloy. *Prog. Nat. Sci.: Mater. Int.* **21**, 380–385 (2011)